Research article

LC-MS-based rheumatoid arthritis serum metabolomics reveals the role of deoxyinosine in attenuating collagen-induced arthritis in mice

Delai Xu [*,1], Liuxing Tang [1], Yueyuan Wang, Jie Pan, Cunjin Su [**]

Department of Pharmacy, the Second Affiliated Hospital of Soochow University, Suzhou, Jiangsu, 215004, China

A R T I C L E   I N F O

A B S T R A C T

Rheumatoid arthritis (RA) is a persistent autoimmune condition with no identified cure currently. Recently, scientists have applied metabolomics to investigate altered metabolic profiles and unique diseases-associated metabolic signatures. Herein, we applied metabolomics approach to analyze serum samples of 41 RA patients and 42 healthy controls (HC) with the aim to characterize RA patients' metabolic profile, investigate related underlying pathological processes, and identify target metabolites. By utilizing ultra-high-performance liquid chromatography coupled with high-resolution mass spectrometry, we found 168 proposed metabolites and 45 vital metabolic pathways. Our analysis revealed that deoxyinosine (DI), a metabolite of the purine metabolic pathway, was the most significant reduced metabolite in RA patients. Furthermore, through targeted detection, we confirmed lower concentration of DI in RA patients' peripheral blood. Moreover, DI inhibited lipopolysaccharide-induced inflammation both *in vitro* and *in vivo*. We further assessed DI's therapeutic potential in a collagen-induced arthritis (CIA) murine model. The results revealed that DI attenuated CIA, as evidenced by significantly lowered clinical scores of arthritis, alleviated joint swelling, and mitigated bone destruction. Moreover, we elucidated the underlying mechanism by which DI increased the population of myeloid-derived suppressor cells (MDSCs) and suppressed the proliferation of induced T cells. Collectively, these findings suggested that DI potentially ameliorated RA by inducing immunosuppressive MDSCs. The study provides key observations on RA pathogenesis and may contribute to developing novel therapeutic strategies for this debilitating condition.

1. Introduction

Rheumatoid arthritis (RA) is a persistent autoimmune condition impacting 0.5-1.0 % of world's population [1]. It is featured by joint inflammation and has the potential to cause irreversible damage and disability. In addition to joint-related complications, RA has been interconnected with augmented risk of cardiovascular diseases, depression, cancer, and other illness. Regrettably, a cure for RA is still elusive [2], and the current focus of treatment is primarily on managing symptoms, relieving pain, and slowing down disease

---

progression. However, given the significant influence of RA on individuals' quality of life, there is an ongoing need for dedicated research efforts to develop effective therapeutic strategies [3].

The primary mechanism driving the pathogenesis of RA is the inflammatory response [4]. Involvement of the cytokines IL-6, IL-17, and TNFα is central to the pathogenesis of RA. These cytokines cause a series of inflammatory response and trigger synovial cell proliferation and cause damage to both cartilage and bone. Studies have demonstrated that blocking inflammatory responses in RA, such as knocking out IL-6, blocking IL-17 with antibodies, or antagonizing TNF-α, can significantly improve inflammatory infiltration and osteoarthrosis in animal models of RA [5–7]. Therefore, identifying new targets or drugs that can inhibit the secretion of inflammatory cytokines and/or suppress inflammatory responses is critical in the treatment of RA.

Significant advancements has been achieved recently in the field of metabolomics applied to RA. Metabolomics have focused on endogenous metabolite analysis and quantification to determine pathological alterations in organisms [8]. Metabolites plays various roles *in vivo*, such as defense, signaling, and interactions with other organisms. Research has revealed the involvement of metabolites in RA-related pathological processes [9,10] and discovered an increasing number of metabolites in the pathogenesis of various diseases [11]. For example, increased sarcosine levels is associated with prostate cancer development, and exogenous sarcosine treatment induces an invasive phenotype in benign prostate epithelial cells [12]. In addition, imidazole which gradually increased with the emergence and progression of RA [13].

The study employed ultra-high-performance liquid chromatography coupled with high-resolution mass spectrometry (UPLC-MS) and performed a nontargeted metabolomic analysis of serum samples of RA patients and HC subjects. Our investigation revealed lower levels of deoxyinosine (DI), an endogenous metabolite involved in the purine metabolic pathway, in RA patients' peripheral blood. Additionally, we utilized a collagen-induced arthritis (CIA) mouse model to assess its inhibitory effect on RA progression and investigated its anti-inflammatory activity and underlying mechanism. Our results collectively indicate that DI suppresses the inflammatory response involved in RA, suggesting that DI could serve as a suitable target for RA treatment.

2. Methods

2.1. Cell culture conditions

RAW264.7 cells were cultivated as a monolayer in DMEM/F12 medium containing 10 % FBS in a humidified incubator at 37 °C with 5 % CO_2.

2.2. RNA isolation and real time quantitative PCR (RT-qPCR)

RNA samples isolated from RAW264.7 cells using the QIAzol reagent were used for RT-qPCR. Briefly, 1 μg RNA was converted into cDNA with oligo (dT) and M-MLV reverse transcriptase and amplified using SYBR Green qPCR Master Mix (Enzynomics, Daejeon) in an ABI QuantStudio 5 device (Applied Biosystems) with primers targeting *iNOS*, *COX-2*, *IL-1β*, *IL-6*, *IL-10*, and *TNF-α*. PCR products were then submitted to horizontal electrophoresis in agarose gels. The primers used in RT-PCR were 5′-TGTAATGAAAGACGGCACACC-3′ and 5′- TCTTCTTTGGGTATT GCTTGG-3′ for *IL-1β*, 5′-TTTGCTTCCATGCTAATGCGAAAG-3′ and 5′- GCTCTGTTGAGGTC-TAAAGGCTCCG-3′ for mouse *iNOS*, 5′- GCGACATACTC AAGCAGGAGCA-3′ and 5′-AGTGGTAACCGCTCAGGTGTTG-3′ for *COX-2*, 5′-TGATGGATGCTACCAAACTGG-3′ and 5′-TTCATGTACTCCAGGTAGCTATGG-3′ for *IL-6*, 5′- AGGCGCTGTCATCGATTT-3′ and 5′-CACCTTGGTCT TGGAGCTTAT-3′ for *IL-10*, and 5′-CTGAGGTCAATCTGCCCAAGTAC-3′ and 5′- CTTCACAGAGCAATGACTCCAAAG-3′ for *TNF-α*.

2.3. Nuclear and cytosolic fractionation

Cells were lysed with a nuclear and cytosol fractionation kit following the manufacturer's instructions. To detect p65, proteins in both fractions were analyzed using Western blot with primary antibodies against p65, histone H3, and GAPDH, as described below.

2.4. Western blot

Cells, treated with or without DI (Sigma-Aldrich, D5287), were washed with ice-cold PBS, collected through centrifugation, and lysed using RIPA buffer with protease/phosphatase inhibitors. The protein content was measured using the bicinchoninic acid protein assay kit. Subsequently, 20 μg of proteins were separated on 12 % SDS-PAGE gels and transferred onto PVDF membranes. Following incubation with 5 % skim milk, the membranes were first reacted with primary antibodies diluted in TBST at 4 °C for 12 h, then with secondary antibodies in TBST for 1 h at 22 °C. The signals were detected using an ECL detection system and quantified using Image-J software. The primary antibodies included anti-COX2 (A5523, Bimake, 1:1000), anti-Nrf2 (16396-1-AP, Proteintech, 1:1000), anti-iNOS (AF0199, Affinity, 1:1000), anti-histone 3 (AF0009, Beyotime, 1:1000), anti-P65 (8242, cst, 1:1000), anti-keap1 (60027-1-Ig, Proteintech, 1:1000), and anti-GAPDH (60004-1-Ig, Proteintech, 1:2000).

2.5. CIA model

All animal experiments were executed by strictly adhering to the guidelines and regulations set by the Ethics Committee of the Second Affiliated Hospital of Soochow University(JD-LK-2022-104-01), China, ensuring the proper care and use of laboratory animals.

Male DBA/1J mice weighing 20–25g and aged 6–8 weeks from Shanghai SLAC Laboratory Animal Company were accommodated in a pathogen-free room with ad libitum access to food and water. After one week of acclimation, mice were randomly assigned into four groups: normal, model, high DI, and low DI, with 12 mice per group. The normal group served as the control, while the other groups were used to establish the CIA mouse model by administering complete Freund adjuvant (Chondrex, 7008) mixed with type II collagen (CII, Chondrex, 20022), followed by a booster injection of incomplete Freund's adjuvant (Chondrex, 7002) mixed with CII on day 21. Starting from day 20 of the experiment, The DI group received 200 mg/kg/d or 500 mg/kg/d DI saline solution through oral administration twice a day for 20 days. The normal and model groups received the same amount of saline. Paw thickness was measured twice or three times per week from the second immunization (day 21) until day 35, the end of the experiment, and arthritis severity was scored accordingly.

2.6. Sepsis mouse model

Sepsis model was established by intraperitoneally injecting lipopolysaccharide (LPS, Sigma-Aldrich, L2280) at 10 mg/kg of body weight (BW) into male BALB/c mice. By comparison, PBS was injected to the control group. To examine the effect of DI, DI saline solution were administered orally to the mice twice a day (200 or 500 mg/kg of BW). The mortality rate was monitored hourly throughout a period of 60 h.

2.7. Mouse primary myeloid-derived suppressor cells (MDSCs)

Mice aged 8–10 weeks were euthanized by cervical dislocation. Mice were immersed in iodophor disinfectant and alcohol for 3 min, then the femur and tibia were separated, and muscles were carefully dissected. The ends of the bones were removed using ophthalmic clippers. The bone marrow was flushed out by rinsing bones and with a 1-mL syringe with 1640 medium. The collected bone marrow was gently combined and centrifuged for 5 min at 1200 rpm. The pellet was gently mixed with 5 mL of erythrocyte lysate, incubated for 5 min at 22–24 °C, centrifuged for 5 min at 1200 rpm, resuspended in RPMI 1640 Medium with 10 % FBS, adjusted to 2×10^6 cells/mL, and cultured in an incubator after adding murine GM-CSF (Novoprotein, CK02) and IL-6 to 10 ng/mL each.

2.8. Isolation of mouse spleen T cells

Spleen of sacrificed mice was removed and place in Hanks' solution. Using a 70-μm sterile nylon screen, the spleen was mechanically disaggregated to obtain a cell suspension and centrifugated for 5 min at 1200 rpm. The pellet was mixed with red cell lysate and centrifuged to collect spleen cells. The cells were redispersed in 100 μL of MACS and sorted using the mouse CD3 immunomagnetic bead kit based on the manufacturer's instructions.

2.9. Flow cytometry assay

The isolated lymphocytes were treated with 100 μL of 3 % FBS-PBS solution containing 1 μL of blocking antibody. After gently shaking at 4 °C for 5–10 min without light, cells were incubated with corresponding antibodies at 4 °C for 15–20 min. After washed with 1 mL of 1 % FBS-PBS solution, cells were centrifuged for 5 min at 200 g, redispersed in 500 μL of 1 % FBS-PBS solution, and analyzed using flow cytometry.

2.10. Micro-computed tomography (micro-CT) analysis

The right ankle joints were soaked in 10 % formalin for 48 h. After one wash with PBS for 2 h and submerged in 75 % ethanol, they were scanned using a micro-CT system (Scanco VIVA CT80, SCANCO Medical AG, Switzerland) with pixel size of 15.6 μm, tube current of 72 μA, tube voltage of 55 kV, and integration time of 200 ms. The cross-sectional images were used to construct a 3D representation of the ankle joints.

The astragalus' bone volume (BV) was determined, and its density was assessed within the range of 370–1000 using the SCANCO Medical μCT software V6.6 (Scanco Medical AG, Switzerland). After that, ankle joints were recreating by reconstructing a stack of 340–441 cross-sections with an inter-section distance of one pixel (15.6 μm) and a height of 5.3-6.9 mm.

3. Ethics statement

The study protocol was pre-approved by the Ethics Committee of the Second Affiliated Hospital of Soochow University (JD-LK-2022-104-01), ensuring compliance with all ethical guidelines. Prior to participating in the study, all enrolled participants provided informed consent.

3.1. Study participants

Between July 2022 and December 2022, 41 RA patients diagnosed based on the criteria used by the American College of Rheumatology in 1987 for RA were included. Concomitantly, 42 HC subjects with matching age, gender, and ethnicity were enrolled as the controls. All participants were Asian descendants recruited from inpatient at the Second Affiliated Hospital of Soochow University.

Table 1 shows the participants' clinical information, including gender, age, C-reactive protein, erythrocyte sedimentation rate, anti-cyclic citrullinated peptide, and rheumatoid factors. The blood samples were collected in coagulating tubes to facilitate clot formation, and serum samples were frozen at −80 °C for subsequent analyses.

3.2. Preparation of serum samples for metabonomics

In this procedure, 100 μL of serum was mixed with 400 μL of methanol in a 1.5-mL tube at −20 °C. After vortexing for 1 min, the sample was spun at 12,000 rpm for 10 min at 4 °C. Subsequently, the supernatant (450 μL) was collected, concentrated by evaporation in an Eppendorf Concentrator (Eppendorf), redissolved in 150 μL of 80 % methanol solution at −20 °C, filtered through a 0.22-μm membrane, and kept at −20 °C for metabolomics analysis.

3.3. UPLC-MS/MS analysis

Sera were analyzed using a Q-Exactive mass spectrometer connected to a UltiMate 3000 UHPLC system (Thermo Scientific) with a Waters Acquity UPLC HSS T3 column (2.1 mm, 17 × 150 mm, 1.8 μm) at 40 °C with autosampler temperature set at 8 °C. The eluents C (water with 0.1 % formic acid) and D (acetonitrile with 0.1 % formic acid) were analyzed under electrospray ionization-positive mode, whereas eluents A (water with 5 mmol/L ammonium formate) and B (acetonitrile) were analyzed under ESI negative (ESI$^-$) mode at 0.25 mL/min and the gradient elution following 2 % eluent D in ESI$^+$ mode or eluent B in ESI$^-$ mode for 1 min followed by linear increase to 50 % over 9 min and to 98 % over 3 min before keeping constant for 1.5 min. Eluent D or B was analyzed at 2 % for 0.5 min and for an additional 6 min before returning to the initial conditions. The mass spectrometer was operated in polarity switching mode (+3.50 kV/-2.5 kV) within an m/z range of 81–1000 by setting the capillary temperature at 325 °C, sheath gas flow at 30 (arbitrary units), auxiliary gas flow at 10 (arbitrary units), full scan resolution at 70,000, and collision voltage at 30 eV. After instrument calibration, a quality control (QC) sample (a mixture of 10 μL of each sample) was analyzed under the specified conditions every five injections to ensure the stability of the UPLC-MS system.

3.4. Data preprocessing

Raw data were transformed and normalized using ProteoWizard (v.3.0.9) and XCMS (v.1.42.0) software based on the retention time, m/z, and intensity. After normalization, only ion peaks with relative relative standard deviations (RSDs) less than 30 % in QC were kept to ensure proper metabolite identification. QC samples realizes data correction and eliminates system errors. SIMCA 14.1 software was employed for principal component analysis (PCA), partial least-squared discriminant analysis (PLS-DA), and orthogonal partial least-squared discriminant analysis (OPLS-DA). The parameters R2X, R2Y, and Q2Y-intercepts were analyzed to confirm the quality of multivariate models and avoid over-fitting. R software package (v.3.3.2) was used for hierarchical cluster analysis. Metabolites with false discovery rate (FDR)≤0.05 and VIP value ≥ 1.0 were selected as changed metabolites. GlobalTest was applied to analyze concentration and examine subtle changes, and relative betweenness centrality was used to determine metabolite importance. The KEGG reference metabolic library were used to create a correlation network using MetaboAnalyst software. Pathway enrichment and topology analyses were performed to recognize the most relevant metabolic pathways in RA.

4. Results

4.1. Differential analysis of serum metabolite profiles of RA patients and HC subjects

To investigate the metabolic profile of RA and its underlying pathological processes and target metabolites, serum samples from 42 HC to 41 RA patients were obtained and analyzed. Table 1 shows participants' information. Herein, the metabolite information of serum samples after pretreatment was analyzed using UPLC-MS/MS method. Fig. 1A and C shows the representative total ion chromatograms (TICs) of serum samples from RA patients and HC. The analytical method was validated using QC and quality assurance (QA), which confirmed the reliability of the cell metabolomics method designed in the present study. Moreover, PCA plot (Fig. 1B and

Table 1
Clinical characteristics of patients with RA and healthy controls. Values are mean ± SD or n (%).

Characteristics	Patients with RA	Healthy
Number of samples	41	42
Age,yrs	59.8 ± 13.6	57.7 ± 11.1
Female	32(78)	34(80)
Disease duration,yrs	6.6 ± 3.1	–
RF, IU/mL	453.9 ± 97	17.5 ± 4.6
ESR, mm/h	43.4 ± 14	9.9 ± 3.2
CRP, mg/L	39.7 ± 15.7	2.5 ± 0.5
Anti-CCP, RU/mL	140.3 ± 97.9	3.9 ± 0.9

RF: rheumatoid factor; ESR: erythrocyte sedimentation rate; CRP: C-reactive protein; anti-CCP: anti-cyclic citrullinated peptide antibodies.
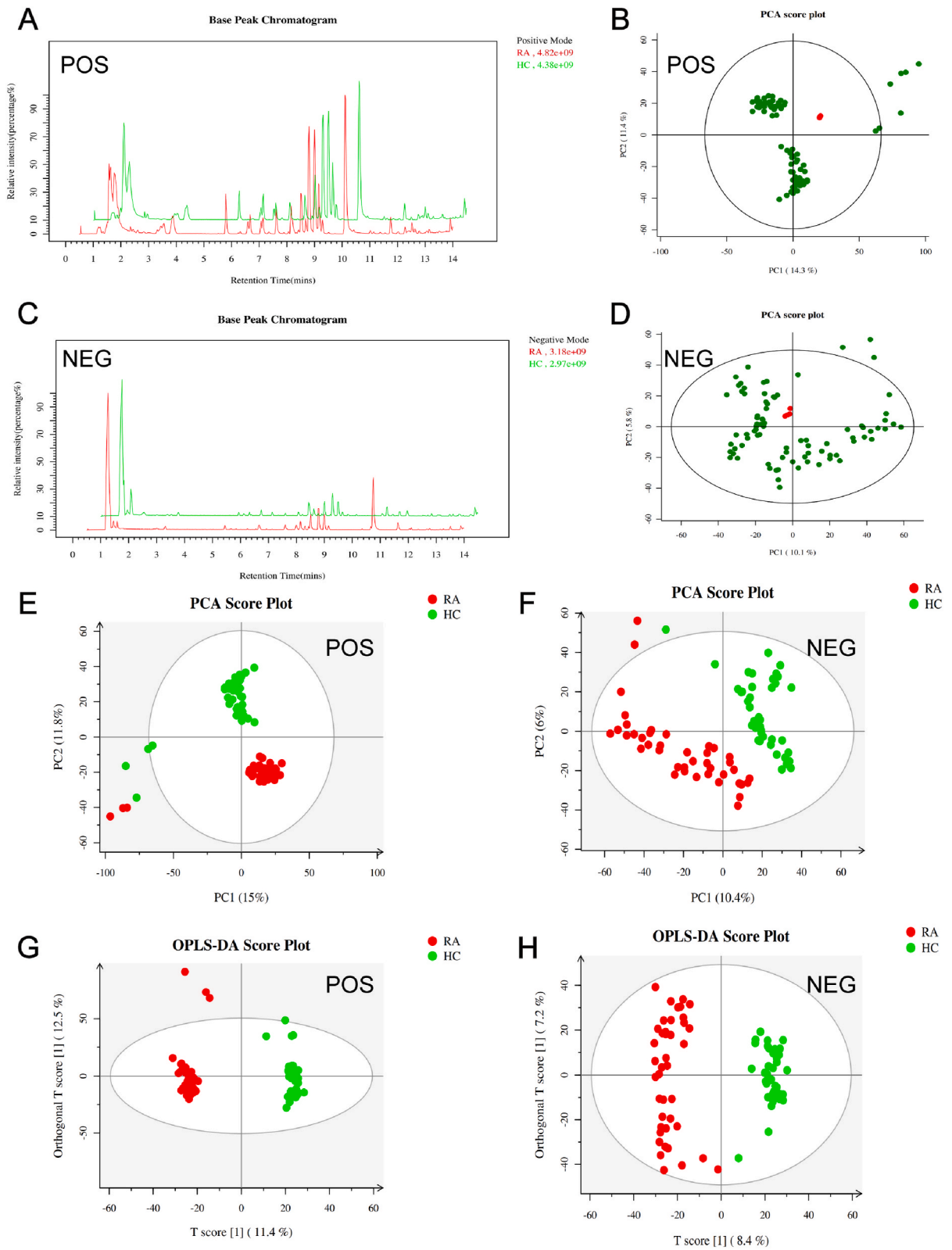
(caption on next page)

Fig. 1. Diagnostic model based on data of serum untargeted metabolomics. (A) Typical base peak ion current chromatograms of samples in positive mode. (B) Principal component analysis (PCA) score plot of quality control (QC) samples clustered together in positive mode. (C) Typical base peak ion current chromatograms of samples in negative mode. (D) PCA score plot with QC samples clustered together in negative mode. (E) PCA score plot of healthy control (HC) and Rheumatic arthritis (RA) samples based on differential metabolites in positive mode. (F) PCA score plot of HC and RA sample groups in negative mode. (G) Orthogonal partial least-squared discriminant analysis (OPLS-DA) score plot of samples in positive mode showing a clearer discrimination between HC and RA sample groups. (H) OPLS-DA score plot of samples in negative mode.

D) depicts a distinct cluster of pooled QC samples, indicating satisfactory stability and repeatability of sample analysis [14]. PCA was used to visualize the differences in metabolic profiles among serum samples. As shown in Fig. 1E and F, HC and RA groups clustered separately, thus indicating that RA patients exhibited a specific metabolic profile which differed from that of HC. OPLS-DA and PLS-DA were conducted to further visualize the differences in metabolite profiles between HC and RA samples [15]. The OPLS-DA score plot (Fig. 1G and H) showed that HC samples clustered separately from RA samples. Taken together, these observations indicated that a clear distinction was found between metabolite profiles of HC and RA samples.

4.2. Identification of differential metabolites between HC and RA subjects

Differential metabolites between HC and RA groups were identified using the OPLS-DA model. The analysis revealed 1828 ions with VIP scores ≥ 1 and $P \leq 0.05$. These metabolites were then subjected to further analysis for chemical structure identification.

The identification process involved two steps. Firstly, each metabolite's precise molecular weight was identified. Secondly, the exact monoisotopic molecular mass was blasted against online databases, including BioDeepDB (www.biodeep.cn/), Mass Bank (www.massbank.jp/), Metlin (http://metlin.scripps.edu/), LipidMaps (www.lipidmaps.org/), Human Metabolome Database (http://www.hmdb.ca/), and mzCloud (www.mzcloud.org/). Table 2 shows the identified 168 metabolites, their names, and the fold change showing their abundance changes. In total, 81 metabolites exhibited significant increase, and 87 metabolites exhibited significant decreases in the RA group compared to the HC group (Table 2).

4.3. Plasma DI levels were significantly decreased in RA

Fig. 2A show the heatmap constructed based on the normalized relative average contents of differential metabolites between the HC and RA groups using MetaboAnalyst 5.0, focusing on the top 20 metabolites based on their VIP values, revealing distinct differences in the abundance of these important metabolites between HC and RA samples.

To deeper understand the functions of identified differential metabolites, we analyzed KEGG metabolic library based on the MetaboAnalyst database and assessed the impact of metabolite profile alteration on pathway functions by changing critical junction points. KEGG analysis identified 45 metabolic pathways based on their P-values (vertical axis) and impact (horizontal axis) that was assessed by the hypergeometric test (Fig. 2B). Correlation analysis to determine the relationships among metabolites found significant changes in linoleic acid metabolism, beta-alanine metabolism, alanine, aspartate, and glutamate metabolism, phenylalanine metabolism, and purine metabolism (Table 3). Among the 168 differential metabolites, DI and xanthine were most influential (Fig. 2C) and involved in purine metabolism. Noteworthy, untargeted metabolomics only allow for semi-quantitative analyses which require further experimental validation and full quantitative analysis. Therefore, we developed a targeted method for measuring DI, which revealed the peak observed in human plasma exhibited identical retention time and fragmentation pattern the synthetic reference substance (Fig. 2D). Subsequently, DI levels were quantified in RA and HC samples using the developed assay. Within these two cohorts, plasma DI levels were higher among the HC subjects (Fig. 2E), indicating a significant reduction in DI level in RA patients and suggesting its importance in the disease. Moreover, methotrexate (MTX), a commonly used medication for RA treatment, had no significant effect on DI concentration in the RA patient blood (Supp.Fig.1).

4.4. DI inhibited LPS-induced inflammation in vitro and in vivo

Previous research has consistently reported lower DI levels among RA patients. Given that RA treatment primarily focuses on anti-inflammatory interventions, it becomes crucial to investigate whether DI possesses anti-inflammatory effects. Inflammation is closely linked to the action of pro-inflammatory IL-1β, TNF-α, and IL-6. Thus, to investigate DI's anti-inflammatory potential, macrophages were treated with LPS to stimulate the release of IL-1β, iNOS, COX2, and TNF-α, thereby mimicking a chronic inflammatory environment, and their levels were determined. Western blotting and RT-qPCR analyses revealed significant elevation in iNOS, COX2, TNF-α, and IL-1β after LPS stimulation, with TNF-α exhibiting the most substantial increase (Fig. 3A–K). However, DI treatment markedly reduced the production of markers involved in LPS-induced inflammation. Noteworthy, both mRNA and protein levels of IL-1β, TNF-α, and COX2 were lower in the LPS group after DI treatment.

NF-κB is a widely expressed nuclear transcription factor with crucial regulatory roles in inflammation. The nucleocytoplasmic shuttling of NF-κB is critical for the transcriptional regulation of target genes. Western blotting analysis showed that DI blocked LPS-induced p65 nuclear translocation (Fig. 3L-N). Sepsis is a life-threatening syndrome associated with systemic inflammatory response. To mimic inflammation *in vivo*, we constructed a sepsis mouse model by intraperitoneally injecting of 10 mg/kg LPS to BALB/c mice and used to evaluate DI's anti-inflammatory effect and prolongation effect on mouse survival rate. The survival curve clearly showed that different doses of DI improved survival rate of mice during sepsis (Fig. 3O). These results indicates that DI effectively attenuates

Table 2
Identified metabolites, their names, and the fold change Table.

Metabolite	VIP	Fold Change CON/DHA	*P*. value	FDR
Deoxyinosine	2.79	0.009	1.3E-14	2.4E-12
Hypoxanthine	2.73	46.697	8.4E-14	6.7E-12
N-Acetylputrescine	2.71	0.035	1.0E-14	4.5E-12
Alpha-Linolenic acid	2.68	14.379	2.5E-13	1.7E-11
2-Ketobutyric acid	2.58	0.319	7.6E-11	2.4E-09
gamma-Glutamylcysteine	2.54	0.618	3.8E-13	2.5E-11
DHEA sulfate	2.53	0.141	9.7E-11	3.0E-09
Isovaleric acid	2.51	0.248	1.1E-11	3.2E-10
ʟ-Glutamic acid	2.43	3.190	2.0E-12	1.0E-10
ʟ-Aspartic acid	2.40	1.824	5.0E-11	1.7E-09
4-Hydroxyphenylpyruvic acid	2.40	17.803	1.8E-13	1.3E-11
Aminoadipic acid	2.31	0.146	7.4E-13	4.4E-11
ᴅ-Mannose	2.28	0.463	7.5E-09	1.3E-07
ʟ-Cystathionine	2.27	0.028	8.4E-14	6.7E-12
Valeric acid	2.13	0.552	1.3E-08	2.1E-07
Pyrrolidonecarboxylic acid	2.12	0.339	2.2E-10	3.3E-09
Uridine	2.11	0.619	9.3E-09	1.6E-07
ʟ-Methionine S-oxide	2.10	0.228	4.7E-11	9.7E-10
9,10-DHOME	2.10	0.578	1.6E-13	1.7E-11
Myristoleic acid	2.09	0.193	3.8E-10	5.1E-09
1-Pyrroline-5-carboxylic acid	2.09	4.107	5.1E-10	6.4E-09
myo-Inositol	2.06	0.526	2.0E-07	2.1E-06
Cortisol	2.05	0.592	2.9E-13	2.4E-11
alpha-Ketoisovaleric acid	2.03	0.665	2.0E-08	3.0E-07
N-Acetylmannosamine	2.01	3.358	1.6E-08	2.5E-07
N(6)-Methyllysine	1.97	3.3419	1.0E-10	1.8E-09
L-4-Hydroxyphenylglycine	1.95	0.43299	7.5E-09	1.3E-07
Malonate	1.94	1.7222	5.1E-07	4.6E-06
2-Heptanone	1.94	4.8328	7.2E-11	1.3E-09
Niacinamide	1.90	2.3397	3.9E-09	3.5E-08
Galactitol	1.89	1.8587	8.6E-11	1.5E-09
Beta-Leucine	1.89	0.20213	1.9E-08	2.8E-07
Mannitol 1-phosphate	1.88	1.8939	1.2E-11	3.4E-10
ʟ-Lactic acid	1.87	1.4035	1.9E-07	2.0E-06
D-Alanyl-ᴅ-alanine	1.86	0.38301	9.4E-07	7.9E-06
Oxoglutaric acid	1.85	1.1531	7.9E-09	6.4E-08
Quassin	1.84	0.18243	1.1E-07	1.3E-06
Isophorone	1.83	0.78913	1.9E-09	1.9E-08
Uracil	1.81	0.29653	3.3E-09	6.5E-08
Androsterone	1.81	0.85146	2.3E-08	1.6E-07
Mandelic acid	1.76	3.2244	1.0E-09	1.1E-08
4-Hydroxycinnamic acid	1.76	2.1638	1.0E-05	6.1E-05
3-Methyl-ʟ-tyrosine	1.74	4.4941	2.7E-11	6.2E-10
12,13-DHOME	1.73	0.40232	1.7E-07	9.4E-07
Hydrogen phosphate	1.72	1.5851	9.0E-06	5.5E-05
1-Pyrroline-2-carboxylic acid	1.69	2.1095	1.4E-07	7.8E-07
Estrone sulfate	1.66	0.20397	1.4E-07	1.6E-06
6-Phosphogluconic acid	1.65	0.55944	1.1E-06	4.8E-06
N-Cyclohexylformamide	1.64	1.6761	8.1E-07	3.8E-06
7-Methylguanine	1.63	1.5799	9.7E-11	1.7E-09
Catechol	1.63	1.1845	8.8E-09	7.0E-08
ʟ-Histidine	1.62	0.40323	2.0E-11	4.9E-10
Pipecolic acid	1.61	1.6833	4.3E-08	2.8E-07
Stearidonic acid	1.60	0.89007	2.7E-07	1.4E-06
4-(Glutamylamino) butanoate	1.60	0.31282	5.3E-07	2.6E-06
2-Amino-3-phosprop	1.58	0.34028	1.2E-06	9.5E-06
Cytosine	1.56	2.0383	2.4E-06	9.9E-06
Decanoyl-ʟ-carnitine	1.55	0.33319	2.9E-07	1.5E-06
1-Methylnicotinamide	1.55	1.5766	9.3E-09	7.3E-08
Pelargonic acid	1.54	4.2588	2.8E-09	2.7E-08
ʟ-Proline	1.54	1.5527	6.4E-09	5.3E-08
Indolebutyric acid	1.53	2.0377	1.4E-07	7.8E-07
N-Acetylleucine	1.51	1.3141	4.1E-09	7.8E-08
Pyroglutamic acid	1.50	1.3362	1.3E-05	7.3E-05
Ribitol	1.50	2.1144	1.4E-06	6.1E-06
3-Hydroxyphenylacetic acid	1.49	4.7732	1.0E-08	8.0E-08
ʟ-Valine	1.48	1.3357	4.0E-07	3.7E-06
ᴅ-Fructose	1.48	0.25615	1.3E-08	9.7E-08

(*continued on next page*)

Table 2 (*continued*)

Metabolite	VIP	Fold Change CON/DHA	*P*. value	FDR
Coniferyl aldehyde	1.47	0.69892	2.6E-08	1.8E-07
13-L-Hydroperoxylinoleic acid	1.47	0.55271	3.5E-06	2.4E-05
Ergothioneine	1.44	0.61607	7.8E-07	3.6E-06
N-Formyl-L-glutamic acid	1.43	0.60244	8.6E-06	3.0E-05
Sodium deoxycholate	1.42	0.60624	2.7E-06	1.1E-05
Sorbitol	1.42	1.4041	1.8E-04	7.1E-04
N-Acetylmuramate	1.42	1.2602	1.2E-06	9.9E-06
Bovinic acid	1.42	0.24934	3.5E-07	3.3E-06
L-Glutamine	1.41	0.73358	1.1E-08	8.4E-08
Hydroxykynurenine	1.39	0.50233	1.0E-04	4.3E-04
cis-1,2-Dihydronaphthalene	1.38	1.557	6.5E-08	4.1E-07
N6-Acetyl-L-lysine	1.38	1.3528	5.8E-05	2.6E-04
Taurine	1.36	3.715	1.4E-07	1.6E-06
2-Hydroxyglutarate	1.35	0.53801	7.9E-05	2.2E-04
Glutathione	1.33	0.16466	9.0E-06	3.1E-05
Ketoleucine	1.33	0.75142	2.4E-05	1.3E-04
1-Methylhistidine	1.31	2.3148	3.5E-05	1.1E-04
3-Methylxanthine	1.31	0.55077	1.8E-04	6.9E-04
Docosapentaenoic acid	1.30	1.717	2.2E-04	5.5E-04
D-Glucose 6-sulfate	1.30	0.29625	1.7E-05	9.3E-05
5-Hydroxytryptophan	1.29	1.835	2.0E-08	1.4E-07
Methylimidazoleacetic acid	1.29	3.0265	6.7E-06	2.4E-05
L-*threo*-3-Phenylserine	1.29	0.41551	1.5E-05	8.6E-05
Dopamine	1.28	0.43842	1.7E-03	4.7E-03
N-Alpha-acetyl lysine	1.28	11.978	6.0E-05	2.7E-04
L-2,4-diaminobutyric acid	1.28	1.417	1.1E-07	6.3E-07
p-Anisic acid	1.27	0.12966	6.4E-09	1.2E-07
Citric acid	1.27	0.70837	4.1E-06	1.6E-05
dGMP	1.27	2.4953	7.9E-03	1.4E-02
D-Sorbose	1.26	2.2075	1.9E-07	1.1E-06
Iminoarginine	1.25	0.70725	6.7E-06	2.4E-05
Acetylphosphate	1.23	0.43971	2.0E-04	5.0E-04
L-Methionine	1.22	1.6626	3.5E-05	1.1E-04
(R)-4-Hydroxymandelate	1.22	0.68256	4.9E-06	1.8E-05
(13E)-11a-Hydroxy-9,15-dioxoprost-13-enoic acid	1.22	1.4003	2.1E-04	5.3E-04
Beta-D-Glucose 6-phosphate	1.22	0.14246	7.9E-04	2.5E-03
Xanthine	1.22	1.8136	2.9E-04	1.1E-03
3,4-Dihydroxymandelic acid	1.22	0.20123	3.1E-05	1.5E-04
Dimethyl sulfone	1.22	0.88835	4.6E-05	1.4E-04
Vanylglycol	1.21	2.0871	7.1E-09	5.8E-08
D-Phenyllactic acid	1.21	1.5354	1.2E-05	3.9E-05
Linoleic acid	1.21	0.78748	4.2E-04	9.8E-04
Guanine	1.20	0.75402	1.5E-06	6.3E-06
5-Acetamidovalerate	1.20	1.5832	2.3E-05	7.4E-05
Dihydrouracil	1.20	0.65162	2.1E-04	5.2E-04
N-Acetylserotonin	1.20	0.47688	4.9E-02	8.5E-02
2-Arachidonoylglycerol	1.20	0.31204	1.3E-08	9.6E-08
Phenylacetylglutamine	1.20	2.6015	4.7E-03	8.7E-03
3,4-Dihydroxyphenylglycol	1.20	0.40065	4.7E-03	1.2E-02
beta-Alanyl-L-lysine	1.19	0.51335	5.5E-04	1.3E-03
D-Gulono-1,4-lactone	1.19	0.32996	5.3E-07	2.6E-06
Undecanoic acid	1.18	0.16865	1.4E-04	5.5E-04
Diethylphosphate	1.18	0.82179	5.7E-04	1.8E-03
2-Oxo-4-methylthiobutanoic acid	1.18	0.4923	1.7E-04	4.4E-04
17a-Estradiol	1.18	0.80574	2.5E-03	6.8E-03
2-Keto-6-aminocaproate	1.18	1.9514	4.5E-04	1.0E-03
Acetylcholine	1.17	1.3925	5.9E-06	2.1E-05
L-Octanoylcarnitine	1.17	0.53385	8.7E-04	1.9E-03
Citramalic acid	1.17	1.383	6.0E-03	1.4E-02
Sphingosine	1.16	1.7355	1.1E-04	3.0E-04
5-Hydroxyindoleacetic acid	1.16	1.6487	1.9E-05	6.1E-05
L-Arabinose	1.16	1.2137	8.2E-05	2.3E-04
N-Acetyl-L-phenylalanine	1.16	1.2893	2.0E-04	7.5E-04
25-Hydroxycholesterol	1.16	0.34256	4.1E-03	1.0E-02
Glucosamine 6-phosphate	1.15	10.531	1.3E-06	7.3E-06
L-Kynurenine	1.12	2.2491	4.9E-06	3.2E-05
Phosphocreatine	1.12	1.9984	7.1E-03	1.6E-02
3-Methylthiopropionic acid	1.12	1.5925	5.4E-05	2.4E-04
Guanosine	1.11	0.75862	8.1E-03	1.8E-02

Table 2 (*continued*)

Metabolite	VIP	Fold Change CON/DHA	*P*. value	FDR
4-Hydroxybenzoic acid	1.10	1.2638	1.6E-09	1.6E-08
cis,cis-Muconate	1.10	2.6633	5.6E-13	3.5E-11
cis-Aconitic acid	1.10	0.75751	2.0E-05	6.4E-05
1H-Indole-3-acetamide	1.09	1.7209	3.8E-07	1.9E-06
Indolelactic acid	1.09	0.7706	4.2E-03	1.0E-02
p-Octopamine	1.09	1.2414	1.4E-05	4.7E-05
Prostaglandin F2a	1.08	0.46923	1.4E-02	2.9E-02
Acetylcholine chloride	1.08	0.86495	4.8E-05	2.2E-04
γ-L-Glutamyl-L-cysteinyl-β-alanine	1.08	1.5612	4.6E-05	1.4E-04
Sphingosine 1-phosphate	1.08	0.74681	1.2E-05	3.9E-05
6-Hydroxyhexanoic acid	1.08	1.4461	7.7E-03	1.8E-02
Butyryl-ʟ-carnitine	1.08	1.582	3.5E-03	6.7E-03
Inosine	1.07	5.0974	5.1E-06	1.9E-05
ʟ-Tyrosine	1.07	1.3173	1.4E-05	4.6E-05
Choline	1.06	1.3462	1.6E-05	5.3E-05
ʟ-Allothreonine	1.06	0.78785	2.7E-05	1.4E-04
dUMP	1.06	0.40218	6.6E-03	1.5E-02
Glucose 6-phosphate	1.06	0.1767	4.6E-04	1.5E-03
Isocitric acid	1.04	1.8242	1.6E-03	3.3E-03
trans-Aconitic acid	1.04	0.81641	4.8E-03	1.2E-02
Prostaglandin E3	1.04	0.24901	8.2E-04	2.5E-03
Retinol	1.03	0.3878	3.6E-05	1.1E-04
Creatinine	1.03	1.8261	1.4E-02	2.9E-02
Creatine	1.02	1.6168	1.9E-03	3.8E-03
Gentisic acid	1.02	2.3769	1.4E-04	3.7E-04
N-[(3a,5b,7a)-3-hydroxy-24-oxo-7-(sulfooxy)cholan-24-yl]-Glycine	1.02	0.41777	3.8E-02	6.9E-02
12-Hydroxydodecanoic acid	1.02	1.182	2.5E-04	6.1E-04
2-Keto-glutaramic acid	1.02	0.60671	9.6E-04	2.1E-03
DMPD	1.01	1.2919	4.8E-05	1.4E-04
ʟ-Arginine	1.01	0.85378	7.6E-05	2.1E-04
Docosahexaenoic acid	1.00	0.51351	1.1E-02	2.3E-02

LPS-induced inflammation *in vitro* and *in vivo*.

4.5. DI alleviates RA in CIA mouse model

To further elucidate DI's therapeutical potential in RA, a CIA model was developed with DBA/1J mice as shown in Fig. 4A. It was revealed that RA was effectively induced in mice after booster immunization on day 21. Moreover, mice in the model group exhibited a slower BW increase compared the control group (Fig. 4B). In addition, paw ankle thickness, paw ankle width, paw volume, and arthritis score were remarkably increased in mice after 14 days (day 35) of booster immunization (Fig. 4C–H), thus indicating the successful establishment of the CIA mouse model. Furthermore, CIA-treated mice were given DI from day 20 via intragastric administration. Moreover, DI administration slowed down the increase in arthritis score in the model group on day 27 (Fig. 4H). Changes in paw ankle thickness and paw ankle width followed a similar trend seen in arthritis scores, continual increase in all groups but beginning to decrease in DI-treated groups from day 30 (Fig. 4D–F). On day 35 (end of the experiment), mice in the DI-treated group exhibited significantly lower arthritis score and decrease in paw ankle thickness and width compared with the model group. Moreover, DI administration dramatically improved spleen weight (Fig. 4I). Histological analysis of joint sections identified severe synovial membrane destruction and hyperplasia and massive inflammatory cell influx into the subsynovial connective tissue in the CIA group. However, mice in DI treatment group exhibited regular articular cartilage, intact synovial membrane, and no inflammatory cell infiltration (Fig. 5A).

It is known that inflammatory bone erosion and destruction are prominent features of RA. Thus, we examined the impacts of DI on CIA-induced bone destruction using micro-CT analysis (Fig. 5B). The micro-CT images of ankle joints revealed distinct differences among the control and experiment groups. The control mice exhibited a clear and smooth structure, while the model mice displayed a destructed bone structure with open porosity. Notably, treatment with DI lead to a significant improvement in bone structure. Specifically, the distal tibias of DI-treated CIA mice exhibited a noteworthy increase in bone volume/tissue volume, trabecular thickness along with a decrease in trabecular number and bone surface/volume ratio when compared to untreated CIA mice (Fig. 5C–F). These findings collectively indicated that DI effectively ameliorate RA in a CIA mouse model.

4.6. DI inhibits T cells by increasing myeloid-derived suppressor cells

Aberrant T cell activation is a known contributing factor in autoimmune diseases, including RA. The effect of DI on T cells from the blood and spleen of CIA mice was interrogated using flow cytometry analysis (Fig. 6A and H). Compared to normal mice, RA mice did not show significant changes in total T cells, CD4$^+$ T cells, and CD8$^+$ T cells in the spleen. However, DI dramatically reduced the precent of CD3$^+$ T cells in RA mouse blood (Fig. 6B) and CD4$^+$ T cells in the blood and spleen (Fig. 6C and J) compared to CIA mice. DI
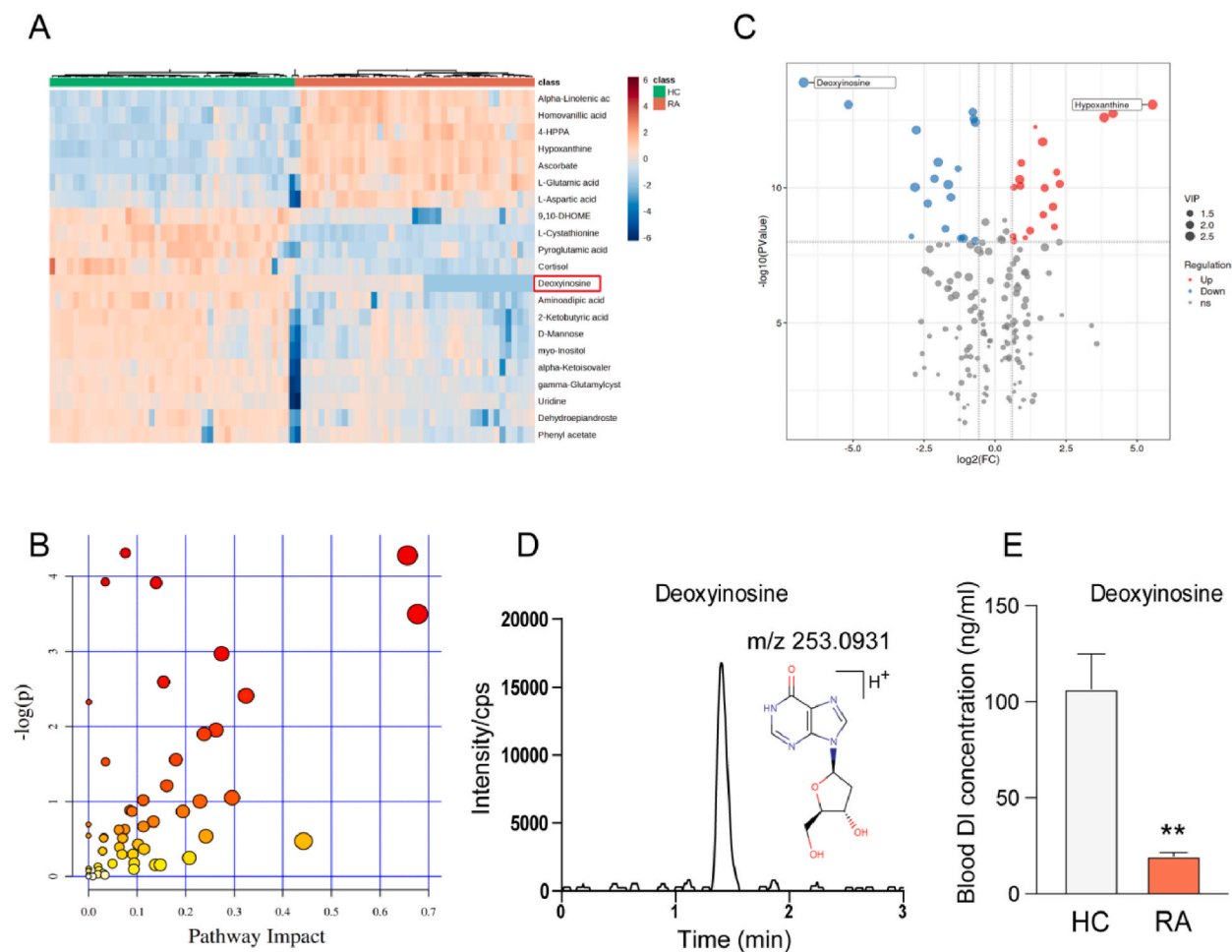
Fig. 2. Metabolite profiling and rheumatic arthritis (RA)-related metabolites. (A) Heatmap of serum samples from healthy control (HC) subjects and RA patients. (B) Enrichment pathway scatter diagram. Most significantly enriched pathways among 45 Kyoto Encyclopedia of Genes and Genomes (KEGG) pathways were determined based on hypergeometric test P values [vertical axis as −log(P); red colored] and impact (horizontal axis; circle diameter). (C) Volcano plots of significantly differential metabolites. (D) Chromatogram of deoxyinosine (DI) in serum samples. (E) Quantification of DI concentration in human serum. P values were calculated using Student's t-test. **$P < 0.01$ vs HC group. n = 4 in healthy control group, n = 4 in RA patients group. (For interpretation of the references to color in this figure legend, the reader is referred to the Web version of this article.)

increased the present of $CD8^+$ T cells both in the blood and spleen (Fig. 6D and K). DI significantly decreased the numbers of $CD3^+$, $CD4^+$, $CD8^+$ T cells in the CIA mice blood (Fig. 6E–G). DI decreased the numbers of $CD4^+$ T cells, but increased the numbers of $CD8^+$ T cells in the CIA mice spleen (Fig. 6L-N).

It has been demonstrated that $CD11b^+Gr\text{-}1^+$ MDSCs is crucial in alleviating inflammation. Herein, flow cytometry analysis results showed the present and number of MDSCs in CIA mice after DI treatment significantly increased in the blood and spleen (Fig. 7A, B, D, E). However, DI had no significant effect on the present and number of dendritic cell in mice spleen (Fig. 7C–F). Moreover, *in vitro* studies confirmed that the stimulation of mouse spleen primary cells with DI treatment induced the increase in M-MDSCs (Fig. 7D and E). Taken together, the above results indicated that DI could increase the number of M-MDSCs.

Subsequently, we examined the proliferation of $CD4^+$ T cells stimulated with anti-CD3/anti-CD28. CCK8 assay showed that DI inhibited $CD4^+$ T cell activation induced by C3/CD28 (Fig. 7F). Therefore, DI treatment led to high levels of $CD11b^+Gr\text{-}1^+$MDSCs, which had a suppressive impact on $CD4^+$ T cells in RA.

5. Discussion

RA is a multifaceted autoimmune condition described by the malfunctioning of various metabolic pathways. It is marked by persistent inflammation in synviall joints and damages to the articular cartilage [16]. Due to its unknown etiology and complex pathogenesis, extensive research on RA is crucial to understand its pathophysiological characteristics and identify potential therapeutic targets [17,18].

Table 3

Correlation analysis to determine the relationships among metabolites.

Pathway	Total	Hits	-Log(P)	impact
Phenylalanine metabolism	45	10	4.3109	0.07563
Linoleic acid metabolism	15	5	4.2799	0.65625
beta-Alanine metabolism	28	7	3.9257	0.03447
D-Glutamine and D-glutamate metabolism	11	4	3.914	0.13904
Alanine, aspartate and glutamate metabolism	24	6	3.4987	0.67712
Pantothenate and CoA biosynthesis	27	6	2.9699	0.27382
Histidine metabolism	44	8	2.5936	0.1546
Arginine and proline metabolism	77	12	2.4106	0.32416
Nitrogen metabolism	39	7	2.326	0.00067
Citrate cycle (TCA cycle)	20	4	1.9541	0.26241
Tyrosine metabolism	76	11	1.8991	0.238
Cysteine and methionine metabolism	56	8	1.5582	0.18007
Glycine, serine and threonine metabolism	48	7	1.5301	0.03491
Valine, leucine and isoleucine biosynthesis	27	4	1.2105	0.16111
Glutathione metabolism	38	5	1.0501	0.2955
Aminoacyl-tRNA biosynthesis	75	9	1.0169	0.11268
Caffeine metabolism	21	3	1.0015	0.22946
Galactose metabolism	41	5	0.88229	0.08543
Lysine biosynthesis	32	4	0.86835	0.0893
Pyrimidine metabolism	60	7	0.86688	0.19428
Sphingolipid metabolism	25	3	0.73141	0.13353
Cyanoamino acid metabolism	16	2	0.69286	0
Ubiquinone and other terpenoid-quinone biosynthesis	36	4	0.66653	0.11305
Phenylalanine, tyrosine and tryptophan biosynthesis	27	3	0.62636	0.07442
Lysine degradation	47	5	0.62102	0.06227
D-Arginine and D-ornithine metabolism	8	1	0.54472	0
alpha-Linolenic acid metabolism	29	3	0.53679	0.24163
Glyoxylate and dicarboxylate metabolism	50	5	0.51983	0.03137
Butanoate metabolism	40	4	0.51112	0.03085
Valine, leucine and isoleucine degradation	40	4	0.51112	0.07013
Taurine and hypotaurine metabolism	20	2	0.47147	0.44245
Riboflavin metabolism	21	2	0.42907	0.10178
Nicotinate and nicotinamide metabolism	44	4	0.39105	0.06335
Ascorbate and aldarate metabolism	45	4	0.36556	0.1143
Propanoate metabolism	35	3	0.3382	0.02893
Fructose and mannose metabolism	48	4	0.2982	0.0912
Purine metabolism	92	8	0.29564	0.0692
Inositol phosphate metabolism	39	3	0.24815	0.20761
Tryptophan metabolism	79	6	0.17747	0.09393
Glycolysis or Gluconeogenesis	31	2	0.17036	0.04924
Pyruvate metabolism	32	2	0.15543	0.13756
Pentose phosphate pathway	32	2	0.15543	0.14775
Primary bile acid biosynthesis	47	3	0.13235	0.01922
Starch and sucrose metabolism	50	3	0.10412	0.00031
Retinol metabolism	22	1	0.095796	0.09322
Glycerophospholipid metabolism	39	2	0.08161	0.0212
Thiamine metabolism	24	1	0.076239	0
Amino sugar and nucleotide sugar metabolism	88	5	0.043574	0.02986
Vitamin B6 metabolism	32	1	0.031022	0.01914
Pentose and glucuronate interconversions	53	2	0.021961	0
Steroid hormone biosynthesis	99	5	0.019418	0.03347
Arachidonic acid metabolism	62	1	0.00111	0.00881
Metabolism of xenobiotics by cytochrome P450	65	1	0.000794	0.00885
Porphyrin and chlorophyll metabolism	104	1	9.90E-06	0

Metabolomics, a branch of science that analyzes endogenous small molecule metabolites using bioinformatics to elucidate changes in organism biology related to biological processes and phenotypes [19,20], has been increasingly employed by researchers in the study of RA [21–23]. Herein, we employed UPLC/MS to analyze changes in metabolite profiles in RA patients. through the analysis, we identified 168 metabolites that exhibited significant differences between the RA and HC groups. Among these differential metabolites, DI group exhibited the most pronounced disparity, with significantly reduced levels, suggesting a potential significant role of DI in RA.

DI is a nucleoside that arises when hypoxanthine is linked to a deoxyribose ring via a beta-N9-glycosidic bond [24]. DI presents naturally in DNA and formed from the conversion of deoxyadenosine catalyzed by adenosine deaminase (ADA) [25]. Individuals with ADA deficiency suffer from severe combined immunodeficiency. Inflammatory conditions lead to increased release of ATP/ADP, which translates to elevated extracellular adenosine and deoxyadenosine levels. Adenosine act as a suppressor of inflammation and we think that low DI levels may be one of the results of RA inflammation. Moreover, DI has been associated with purine nucleoside phosphorylase (PNP) deficiency, an inborn metabolic error [26].
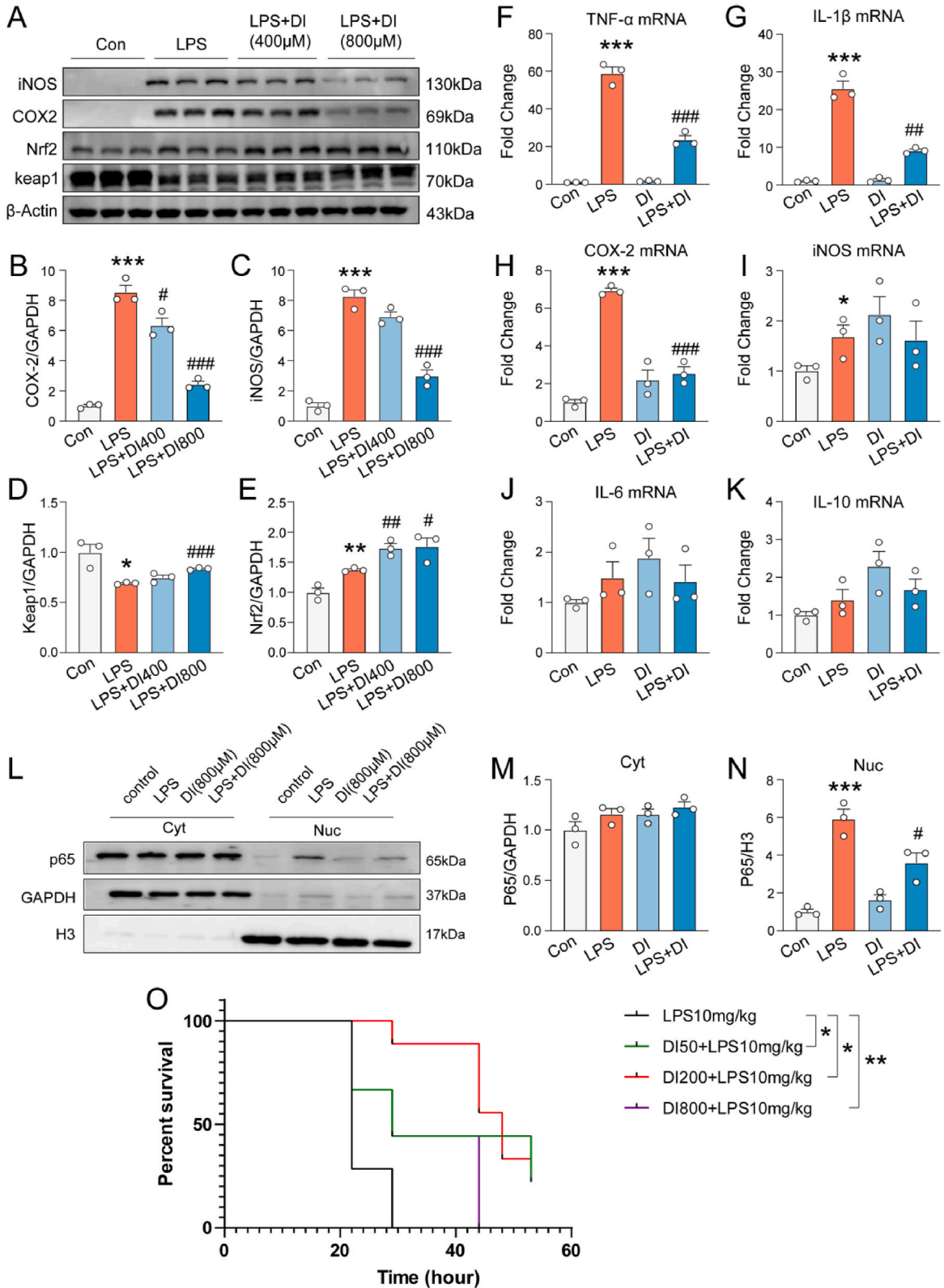
(caption on next page)

Fig. 3. Deoxyinosine (DI) inhibits LPS-induced inflammation in vitro and in vivo. Raw 264.7 cells were pretreated with 400 μM or 800 μM DI for 30 min, and then were treated with 10 ng/ml LPS for 6 h. (A) iNOS, COX2, NRF2, and keap1 determined by Western blot. (B–E) Quantification of iNOS, COX2, Nrf2, and keap1. (F–K) mRNA levels of TNF-α, IL-1β, COX2, iNOS, IL-6, and IL-10 determined by qPCR in different treatment groups. (L) Inhibitory effect of DI on P65 nuclear transposition determined by immunoblot analysis of subcellular fractionated samples. (M–N) Quantification of p65 in cytoplasm and nucleus. *p < 0.05, **p < 0.01, ***p < 0.001 vs control group, #p < 0.05, ##p < 0.01, ###p < 0.001 vs LPS group. n = 3. P values were calculated using One-way ANOVA method. (O) Survivorship curve of septic mice after DI treatment. *p < 0.05, **p < 0.01 vs LPS group. p values were calculated by Kaplan-Meier analysis method.
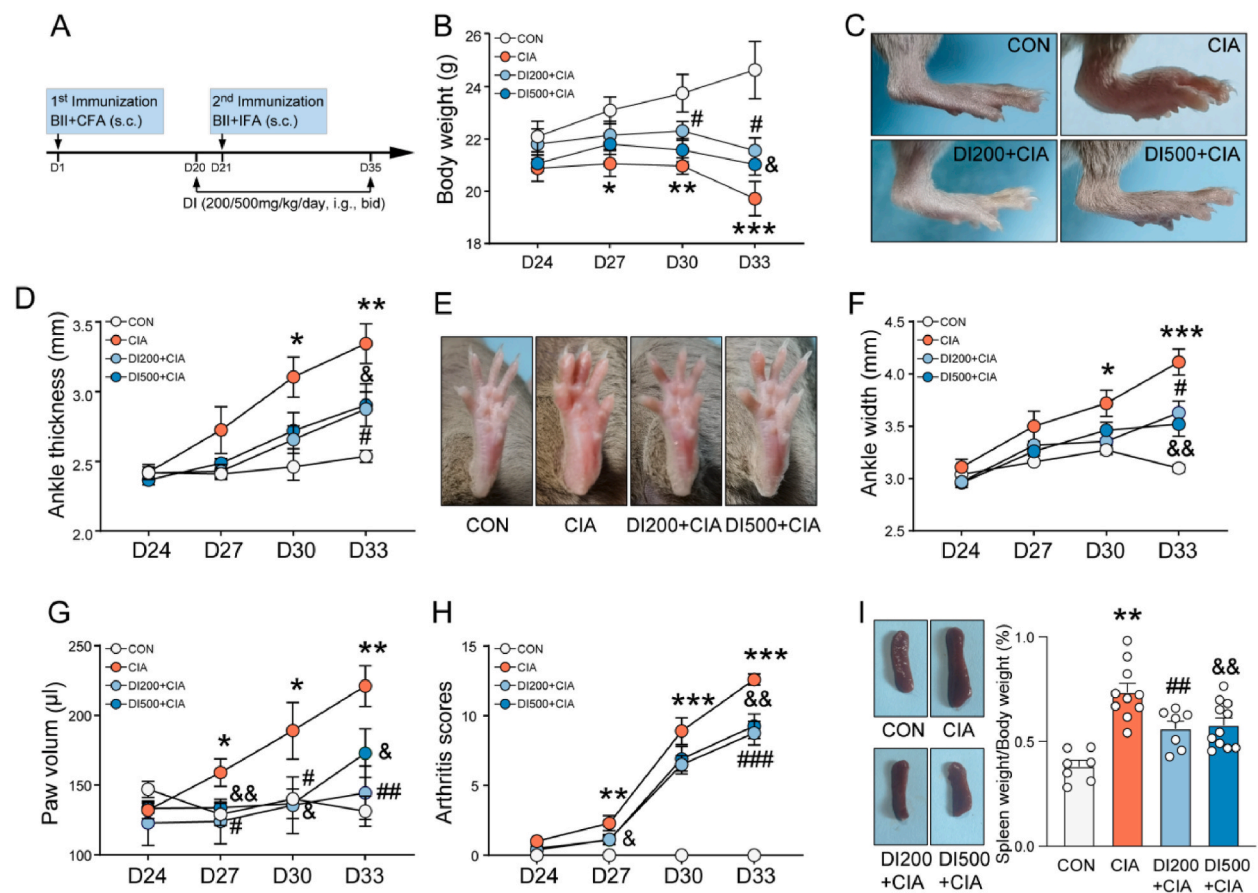
Fig. 4. Effect of deoxyinosine (DI) treatment on collagen-induced arthritis (CIA) in mice. (A) Timeline scheme of experiments. CIA model was established with initial immunization on day 1 and booster immunization on day 21. DI was administered orally twice a day from day 20 to the day prior (day 35) to the end of the experiment. (B) Body weight. (C, D) Changes in ankle thickness. (E, F) Changes in ankle width. (G) Changes in paw volume. (H) Arthritis score. (I) Spleen weight. *p < 0.05, **p < 0.01, ***p < 0.001 vs control group. #p < 0.05, ##p < 0.01, ###p < 0.001 vs CIA group; &p < 0.05, &&p < 0.01 vs CIA group. P values were calculated by One-way ANOVA method. n = 7 in control group, n = 10 in CIA group, n = 7 in DI200 group, n = 11 in DI500 group.

Previous studies have suggested that blocking NF-kB pathways is crucial for managing inflammatory responses in RA [27,28]. NF-κB is essential for modulating the production of pro-inflammatory cytokines and enzymes associated with inflammatory process. Thus, NF-κB is considered a major therapeutic target for various diseases. It is well established that blocking NF-κB transcriptional activity in the nucleus of macrophages can effectively suppress pro-inflammatory IL-1β, IL-6, and TNF-α as well as enzymes like iNOS and COX-2 [29]. Given the positive correlation between inflammatory response and the severity of RA [27], LPS was used herein to stimulate macrophages to mimic macrophage activation during RA. It was shown that DI inhibited LPS-induced transposition of NF-κB p65 subunit in RAW264.7 macrophages. Therefore, blocking NF-κB pathways in macrophages by DI may downregulate pro-inflammatory mediators, thus leading to an anti-inflammatory effect *in vitro*.

Sepsis is a life-threatening disease that often causes multiple organ failure primarily as a result of an uncontrolled inflammatory response [30]. The septic response is featured by elevated levels of inflammatory TNF-α, IL-1β, and IL-6, as well as COX-2 and NO [31]. LPS, a component of Gram-negative bacteria, could stimulate host cells to produce pro-inflammatory cytokines, causing acute inflammation. Herein, we established a sepsis mouse model using LPS to evaluate the *in vivo* anti-inflammatory effect of DI at different doses. It was demonstrated that DI prolonged the survival time of septic mice, thus suggesting an anti-inflammatory effect of DI.
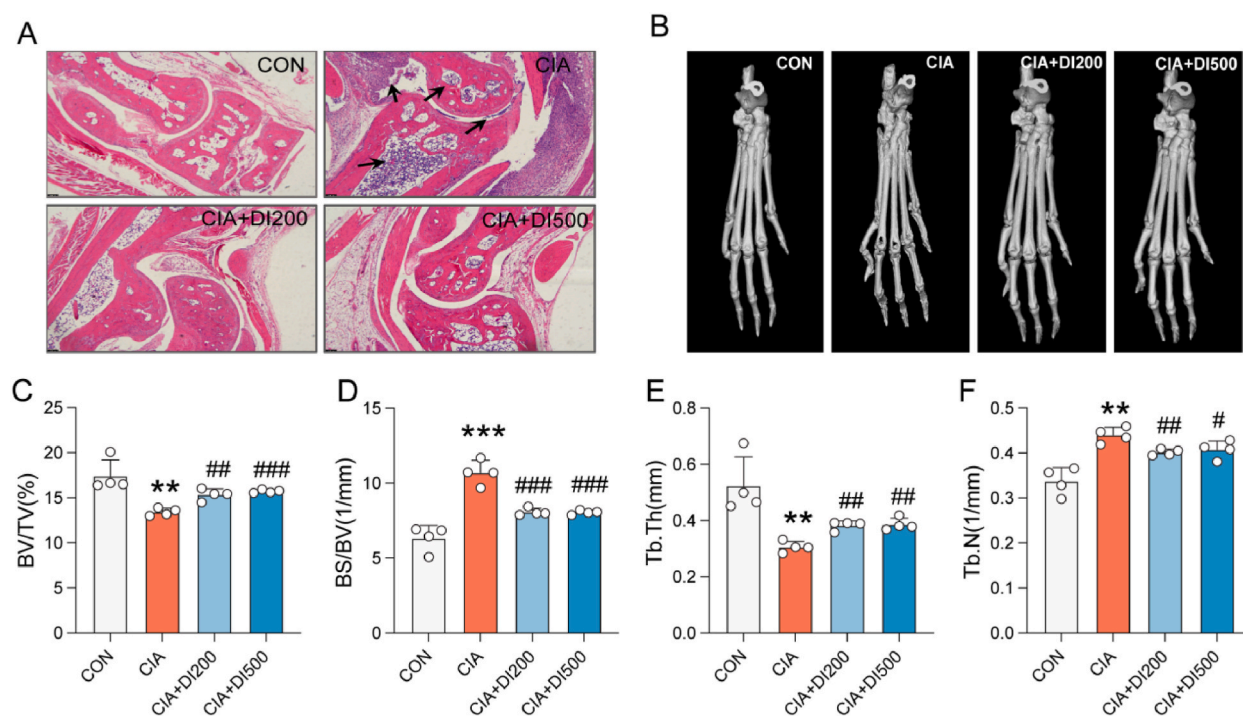
Fig. 5. Deoxyinosine (DI) prevents joint destruction in a collagen-induced arthritis (CIA) model. (A) Images of ankle joint of CIA mice after hematoxylin-eosin (H&E) staining. (B) Micro-computed tomography (Micro-CT) images of metapedes. (C–F) BV/TV, BS/BV, Tb Th, and Tb N in the distal tibia of mice were determined by micro-CT. **$p < 0.01$, ***$p < 0.001$ vs control group, and #$p < 0.05$, ##$p < 0.01$, ###$p < 0.001$ vs CIA group. P values were calculated by One-way ANOVA method. n = 4.

The CIA mouse model is commonly used to study RA [32]. Consistent with previous reports [33], our data showed that DI could effectively attenuate CIA, as demonstrated by the alleviation of RA-related symptoms, including synovial hyperplasia, inflammatory cell infiltration, bone destruction, and cartilage erosion, combined with a reduction in arthritis score, paw thickening and recovered joint bone structure. Abnormal T cell activation and the subsequent persistent inflammatory response play a crucial role in RA development [34]. Among various T cells, CD4^{+} T cells can differentiate into pro-inflammatory effector cells and contribute significantly to the immune cell infiltration in the synovium [35]. In the context of compromised T cell tolerance due to defective DNA repair, the presence of DI in DNA may be relevant.

Furthermore, our animal experiments revealed that DI significantly reduced the abundance of CD4^{+} T cells in mouse spleen and blood. Notably, the abundance of MDSCs in the blood and spleen of mice treated with DI significantly increased. MDSCs are an important class of immunosuppressive cells that inhibit the activity of T cells and exert an immunosuppressive effect [36]. Targeting MDSCs has shown promise in the treatment of autoimmune diseases [37,38]. Our results showed that DI alleviated disease activity in the CIA model likely by increasing the number of MDSCs and suppressing abnormal CD4^{+} T cells activation, thereby alleviating the inflammatory response. These findings are in line with other reports [39] that emphasize the critical role of MDSCs in inhibiting T cell proliferation both *in vitro* and *in vivo*. Thus, DI may exert its impacts on inflammatory T cells directly as well as indirectly through MDSCs.

6. Conclusions

Herein, we comprehensively analyzed the serum metabolite profiles of RA patients using UPLC-MS analysis, which revealed a significant reduction in DI levels in RA patients compared to HC. Considering that inflammation is an important etiological factor in RA, our findings suggest that the therapeutical effect of DI in attenuating CIA in a mouse model is likely attributed to its ability to target anti-inflammatory pathways. This potential anti-inflammatory activity of DI may be crucial in explaining its deficiency in RA patients. Furthermore, our experiments revealed that exogenous supplementation of DI can enhance anti-inflammatory MDSCs and decrease pro-inflammatory cytokines, indicating that DI plays a role in restoring normal immune function in RA patients. Our results provide valuable evidence supporting the benefitial potential of DI in the treatment of RA. However, determining the clinical application value of DI requires further evaluation and optimization.
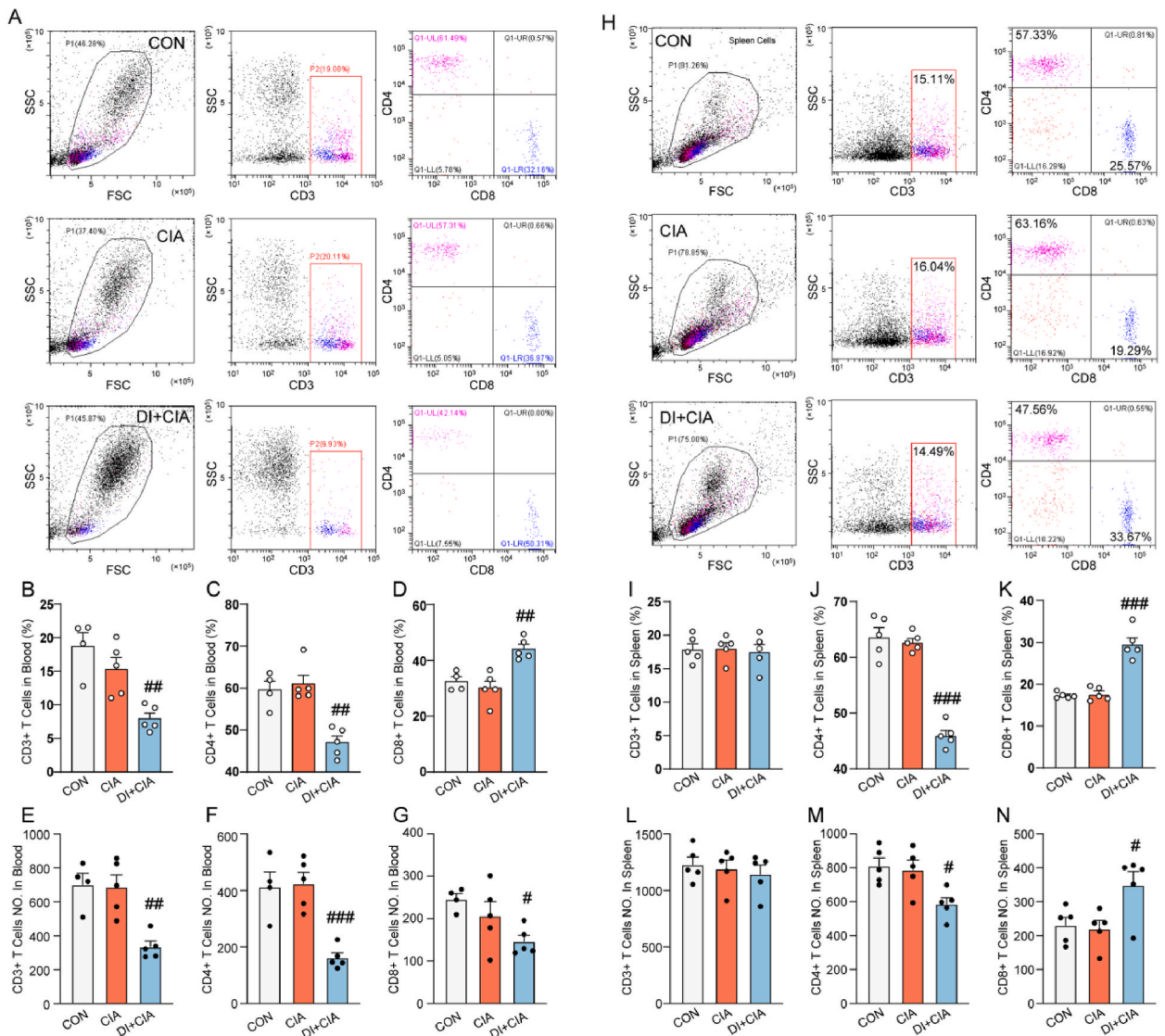
Fig. 6. Effect of deoxyinosine (DI) on T cells. (A, H)The representative staining of T cells ($CD3^+/CD4^+/CD8^+$) of blood and spleen were determined by flow cytometry. The representative percentage (B–D) and the numbers (E–G) of T cells in the Blood. The representative percentage (I–K) and the numbers (L–N) of T cells in the spleen. #$p < 0.05$, ##$p < 0.01$, ###$p < 0.001$ vs CIA group. P values were calculated by One-way ANOVA method. n = 4–5.

Data availability statement

Data included in article/supp. material/referenced in article.

CRediT authorship contribution statement

Delai Xu: Writing – review & editing, Writing – original draft, Conceptualization. **Liuxing Tang:** Conceptualization. **Yueyuan Wang:** Methodology, Investigation. **Jie Pan:** Project administration. **Cunjin Su:** Writing – review & editing, Software, Conceptualization.

Declaration of competing interest

The authors declare that they have no known competing financial interests or personal relationships that could have appeared to influence the work reported in this paper.
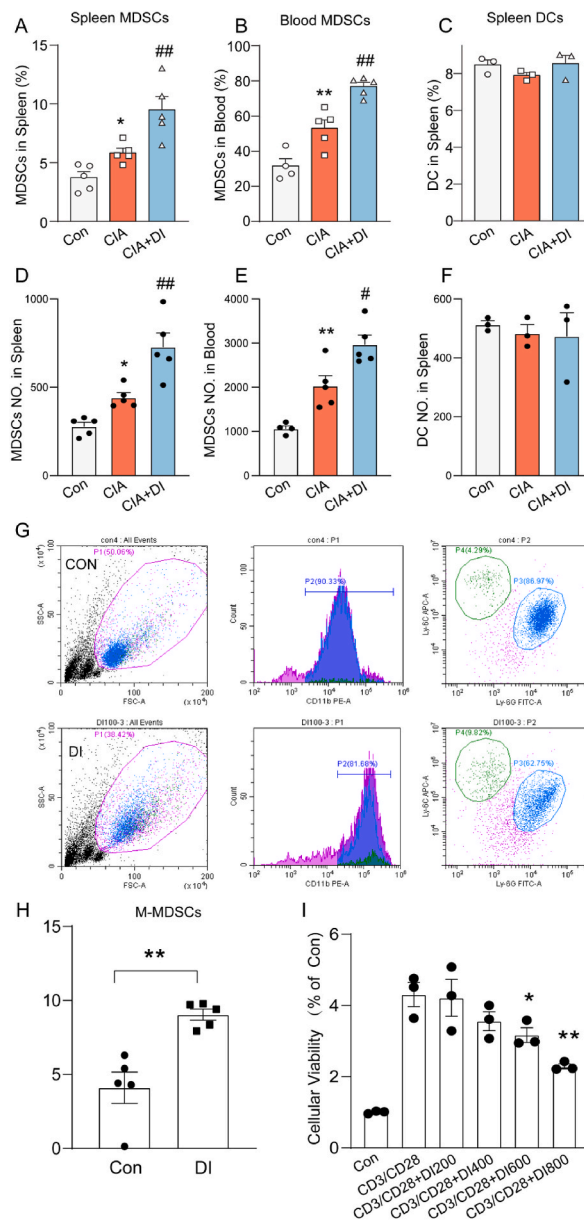
Fig. 7. DI treatment induced the increase in MDSCs. (A, B) The representative percentage (D, E) and the number of MDSCs of the blood and spleen were determined by flow cytometry. (C) The representative percentage (F) and the number of dendritic cell of spleen. *p < 0.05, **p < 0.01 vs control group, #p < 0.05, ##p < 0.01 vs the CIA group. P values were calculated by One-way ANOVA method. n = 3. (G, H) The representative staining of MDSCs of mouse spleen primary cells with DI treatment *in vitro*. **p < 0.01 vs control group. P values were calculated by *t*-test. n = 5. (I) T cells isolated from mice spleen were stimulated with CD3/CD28 (2 μg/ml, 100 μL/well, coated overnight). CCK8 assay showed that DI inhibited T cell activation induced by CD3/CD28. *p < 0.05, **p < 0.01 vs CD3/CD28 group. P values were calculated by One-way ANOVA method. n = 3.

Appendix A. Supplementary data

Supplementary data to this article can be found online at https://doi.org/10.1016/j.heliyon.2024.e30903.

References

[1] M.H. Smith, J.R. Berman, What is rheumatoid arthritis? JAMA 327 (12) (2022) 1194.

[2] D. Aletaha, J.S. Smolen, Diagnosis and management of rheumatoid arthritis: a review, JAMA 320 (13) (2018) 1360–1372.

[3] G. Schett, Y. Tanaka, J.D. Isaacs, Why remission is not enough: underlying disease mechanisms in RA that prevent cure, Nat. Rev. Rheumatol. 17 (3) (2021) 135–144.

[4] J.S. Smolen, D. Aletaha, I.B. Mcinnes, Rheumatoid arthritis, Lancet (London, England) 388 (10055) (2016) 2023–2038.

[5] T. Kishimoto, S. Kang, IL-6 revisited: from rheumatoid arthritis to CAR T cell therapy and COVID-19, Annu. Rev. Immunol. 40 (2022) 323–348.

[6] S.P.D. Berry, C. Dossou, A. Kashif, et al., The role of IL-17 and anti-IL-17 agents in the immunopathogenesis and management of autoimmune and inflammatory diseases, Int. Immunopharm. 102 (2022) 108402.

[7] N. Biesemann, D. Margerie, C. Asbrand, et al., Additive efficacy of a bispecific anti-TNF/IL-6 nanobody compound in translational models of rheumatoid arthritis, Sci. Transl. Med. 15 (681) (2023) eabq4419.

[8] Z. He, Z. Liu, L. Gong, Biomarker identification and pathway analysis of rheumatoid arthritis based on metabolomics in combination with ingenuity pathway analysis, Proteomics 21 (11–12) (2021) e2100037.

[9] D. Yu, J. DU, X. Pu, et al., The gut microbiome and metabolites are altered and interrelated in patients with rheumatoid arthritis, Front. Cell. Infect. Microbiol. 11 (2021) 763507.

[10] L. Song, Q. Yin, M. Kang, et al., Untargeted metabolomics reveals novel serum biomarker of renal damage in rheumatoid arthritis, J. Pharmaceut. Biomed. Anal. 180 (2020) 113068.

[11] T.J. Wang, M.G. Larson, R.S. Vasan, et al., Metabolite profiles and the risk of developing diabetes, Nat. Med. 17 (4) (2011) 448–453.

[12] A. Sreekumar, L.M. Poisson, T.M. Rajendiran, et al., Metabolomic profiles delineate potential role for sarcosine in prostate cancer progression, Nature 457 (7231) (2009) 910–914.

[13] J.H. Koh, S.J. Yoon, M. Kim, et al., Lipidome profile predictive of disease evolution and activity in rheumatoid arthritis, Exp. Mol. Med. 54 (2) (2022) 143–155.

[14] W.B. Dunn, D. Broadhurst, P. Begley, et al., Procedures for large-scale metabolic profiling of serum and plasma using gas chromatography and liquid chromatography coupled to mass spectrometry, Nat. Protoc. 6 (7) (2011) 1060–1083.

[15] E.A. Th Venot, A. Roux, Y. Xu, et al., Analysis of the human adult urinary Metabolome variations with age, body mass index, and gender by implementing a comprehensive workflow for univariate and OPLS statistical analyses, J. Proteome Res. 14 (8) (2015) 3322–3335.

[16] Y.J. Lin, M. Anzaghe, L.K.E.S. Sch, Update on the pathomechanism, diagnosis, and treatment options for rheumatoid arthritis, Cells 9 (4) (2020).

[17] G.R. Burmester, J.E. Pope, Novel treatment strategies in rheumatoid arthritis, Lancet (London, England) 389 (10086) (2017) 2338–2348.

[18] J.A. Singh, Treatment guidelines in rheumatoid arthritis, Rheum. Dis. Clin. N. Am. 48 (3) (2022) 679–689.

[19] C. Jang, L. Chen, J.D. Rabinowitz, Metabolomics and isotope tracing, Cell 173 (4) (2018) 822–837.

[20] C.H. Johnson, J. Ivanisevic, G. Siuzdak, Metabolomics: beyond biomarkers and towards mechanisms, Nat. Rev. Mol. Cell Biol. 17 (7) (2016) 451–459.

[21] L. Xu, C. Chang, P. Jiang, et al., Metabolomics in rheumatoid arthritis: advances and review, Front. Immunol. 13 (2022) 961708.

[22] N. Yoon, A.K. Jang, Y. Seo, et al., Metabolomics in autoimmune diseases: focus on rheumatoid arthritis, systemic lupus erythematous, and multiple sclerosis, Metabolites 11 (12) (2021).

[23] C. Li, B. Chen, Z. Fang, et al., Metabolomics in the development and progression of rheumatoid arthritis: a systematic review, Joint Bone Spine 87 (5) (2020) 425–430.

[24] C.C. Lee, Y.C. Yang, S.D. Goodman, et al., Deoxyinosine repair in nuclear extracts of human cells, Cell Biosci. 5 (2015) 52.

[25] S. Signa, A. Bertoni, F. Penco, et al., Adenosine deaminase 2 deficiency (DADA2): a crosstalk between innate and adaptive immunity, Front. Immunol. 13 (2022) 935957.

[26] G. LA Marca, E. Giocaliere, S. Malvagia, et al., Development and validation of a 2nd tier test for identification of purine nucleoside phosphorylase deficiency patients during expanded newborn screening by liquid chromatography-tandem mass spectrometry, Clin. Chem. Lab. Med. 54 (4) (2016) 627–632.

[27] D.D. Ilchovska, D.M. Barrow, An Overview of the NF-kB mechanism of pathophysiology in rheumatoid arthritis, investigation of the NF-kB ligand RANKL and related nutritional interventions, Autoimmun. Rev. 20 (2) (2021) 102741.

[28] L. An, Z. Li, L. Shi, et al., Inflammation-targeted celastrol nanodrug attenuates collagen-induced arthritis through NF-κB and Notch 1 pathways, Nano Lett. 20 (10) (2020) 7728–7736.

[29] S. Wang, M. Lu, W. Wang, et al., Macrophage polarization modulated by NF-κB in polylactide membranes-treated peritendinous adhesion, Small 18 (13) (2022) e2104112.

[30] D.C. Angus, T. Van Der Poll, Severe sepsis and septic shock, N. Engl. J. Med. 369 (9) (2013) 840–851.

[31] P. Raeven, J. Zipperle, S. Drechsler, Extracellular vesicles as markers and mediators in sepsis, Theranostics 8 (12) (2018) 3348–3365.

[32] D.D. Brand, K.A. Latham, E.F. Rosloniec, Collagen-induced arthritis, Nat. Protoc. 2 (5) (2007) 1269–1275.

[33] H. Malhotra, V. Garg, G. Singh, Biomarker approach towards rheumatoid arthritis treatment, Curr. Rheumatol. Rev. 17 (2) (2021) 162–175.

[34] C.M. Weyand, J.J. Goronzy, The immunology of rheumatoid arthritis, Nat. Immunol. 22 (1) (2021) 10–18.

[35] A.H.S. Heng, C.W. Han, C. Abbott, et al., Chemokine-driven migration of pro-inflammatory CD4(+) T cells in CNS autoimmune disease, Front. Immunol. 13 (2022) 817473.

[36] S. Hegde, A.M. Leader, M. Merad, MDSC: markers, development, states, and unaddressed complexity, Immunity 54 (5) (2021) 875–884.

[37] F. Veglia, E. Sansiviero, D.I. Gabrilovich, Myeloid-derived suppressor cells in the era of increasing myeloid cell diversity, Nat. Rev. Immunol. 21 (8) (2021) 485–498.

[38] D. Xu, C. Li, Y. Xu, et al., Myeloid-derived suppressor cell: a crucial player in autoimmune diseases, Front. Immunol. 13 (2022) 1021612.

[39] T. Baumann, A. Dunkel, C. Schmid, et al., Regulatory myeloid cells paralyze T cells through cell-cell transfer of the metabolite methylglyoxal, Nat. Immunol. 21 (5) (2020) 555–566.